



A twenty year record of greenhouse gases in the Eastern Mediterranean atmosphere



Nikos Gialesakis^a, Nikos Kalivitis^a, Giorgos Kouvarakis^a, Michel Ramonet^b, Morgan Lopez^b, Camille Yver Kwok^b, Clement Narbaud^b, Nikos Daskalakis^c, Marios Mermigkas^d, Nikolaos Mihalopoulos^{a,e}, Maria Kanakidou^{a,c,f,*}

^a Environmental Chemical Processes Laboratory, Department of Chemistry, University of Crete, 70013 Heraklion, Greece

^b Laboratoire des Sciences du Climat et de l'Environnement (LSCE), IPSL, CEA-CNRS-UVSQ, Université Paris-Saclay, Gif-sur-Yvette, France

^c Laboratory for Modeling and Observation of the Earth System (LAMOS), Institute of Environmental Physics (IUP), University of Bremen, Bremen, Germany

^d Department of Physics, Aristotle University of Thessaloniki, Greece

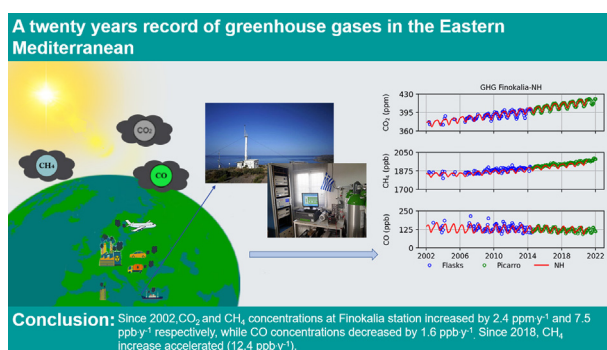
^e Institute for Environmental Research and Sustainable Development (IERSD), National Observatory of Athens, Penteli, Greece

^f Center of Studies on Air quality and Climate Change (CSTACC), ICE-HT/FORTH, Patras, Greece

HIGHLIGHTS

- Eastern Mediterranean atmospheric CO₂ and CH₄ are increasing while CO is decreasing.
- CH₄ levels are higher than the Northern hemisphere mean indicating regional sources
- CO seasonality presents a secondary summertime maximum attributed to wildfires
- CH₄ and CO mean summertime diurnal cycles are consistent with oxidation by OH

GRAPHICAL ABSTRACT



ARTICLE INFO

Editor: Pavlos Kassomenos

Keywords:

Eastern Mediterranean atmosphere
Greenhouse gases
Carbon dioxide
Methane
Carbon monoxide
Trends

ABSTRACT

Twenty years of CO₂, CH₄ and CO greenhouse gas atmospheric concentration measurements at Finokalia station on Crete in the Eastern Mediterranean region are presented. This dataset is the longest in the Eastern Mediterranean, based on bi-weekly grab sampling since 2002 and continuous observations since June 2014. CO₂ concentrations increase by 2.4 ppm·y⁻¹ since 2002, in agreement with the general north hemisphere trend as derived by worldwide NOAA observations. CH₄ showed a mean increasing trend of 7.5 ppb·y⁻¹ since 2002, a rate that has accelerated since 2018 (12.4 ppb·y⁻¹). In contrast, CO has decreased by 1.6 ppb·y⁻¹ since 2002, which resulted from a strong decrease until 2017 (2.5 ppb·y⁻¹), followed by a small increase in the last 3 years (0.2 ppb·y⁻¹). Both CO₂ and CH₄ present maxima during winter and minima during summer, in general agreement with the observations at the ICOS stations in Europe. CO also presents the highest values in winter and the lowest values in summer during June, while a secondary maximum is seen in August, which can be attributed to open fires that often occur in the area during this period. The mean summertime diurnal cycles of CH₄ and CO agree with a 24-h mean OH radical concentration of the order of 0.3–1 × 10⁷ molecules·cm⁻³ over the region, in general agreement with the only existing in-situ observations at Finokalia for 2001.

1. Introduction

Global warming has severe impacts on economy, security and human health (Stern, 2007). The rapid human-driven increase of greenhouse gas

* Corresponding author at: Environmental Chemical Processes Laboratory, Department of Chemistry, University of Crete, 70013 Heraklion, Greece.
E-mail address: mariak@uoc.gr (M. Kanakidou).

(GHG) is the main responsible factor for the global temperature increase, due to GHG's ability to absorb the infrared radiation. This impact has increased during the last decade: the last 8 years (2013 to 2021) as well as the years 2005 and 2010 are among the warmest ten years since 1880. Regionally, in climate sensitive areas, like the Arctic and the Mediterranean, temperature changes can be faster than the global mean. In particular, data analysis in Zittis et al. (2022) has shown that the Eastern Mediterranean and Middle East region warmed about two times faster than the global average temperature increase (0.45 °C/decade versus 0.27 °C/decade globally) for the period 1981–2019. This faster warming is found to be characteristic of the last 2 decades, since accounting for the entire 20th century (1901–2019) the two trends, regional and global, are very similar. The rise of the average temperature has been accompanied by more frequent extreme weather features, e.g. heatwaves, droughts, heavy rains (Zittis et al., 2022). According to the IPCC sixth assessment report (IPCC, 2022) CO₂ and CH₄ contribute approximately 53 % and 34 % respectively to the global warming by GHG (CO₂, CH₄, N₂O and CFCs) from 1750 to 2011.

Carbon dioxide's lifetime in the atmosphere is controlled by its uptake by the ocean, $2.8 \pm 0.4 \text{ GtC}\cdot\text{y}^{-1}$, and terrestrial vegetation, $3.1 \pm 0.6 \text{ GtC}\cdot\text{y}^{-1}$, according to the 2021 Global Carbon Budget for the decade 2011–2020 (Friedlingstein et al., 2022), and is of the order of a few hundreds of years (Forster et al., 2007). The primary sources of CO₂ are fossil fuel combustion and cement production ($9.5 \pm 0.5 \text{ GtC}\cdot\text{y}^{-1}$) and land use emissions mainly due to deforestation ($1.5 \pm 0.7 \text{ GtC}\cdot\text{y}^{-1}$). Carbon dioxide levels have increased rapidly since the beginning of the Industrial Era, from approximately 277 ppm (10^{-6} v/v) in 1750 (Joos and Spahni, 2008) to 412.5 ppm in 2020 (Friedlingstein et al., 2022).

Methane has a mean lifetime of 9.8 ± 1.6 years (Voulgarakis et al., 2013) that is at least one order of magnitude shorter than that of CO₂. Despite being significantly less prevalent in the atmosphere than CO₂, methane absorbs thermal infrared radiation far more efficiently and hence has a global warming potential (GWP) that is 86 times higher per unit mass on a 20-year timescale, and 28 times stronger on a 100-year timescale, than CO₂ (Jackson et al., 2020). The primary sources of CH₄ are emissions from fossil fuel use ($111\text{--}128 \text{ Tg CH}_4\cdot\text{y}^{-1}$), from agriculture and waste management ($206\text{--}217 \text{ Tg CH}_4\cdot\text{y}^{-1}$), from biomass and bio-fuel burning ($30 \text{ Tg CH}_4\cdot\text{y}^{-1}$), from wetlands ($149\text{--}181 \text{ Tg CH}_4\cdot\text{y}^{-1}$) and other natural emissions, including permafrost and termites ($37\text{--}222 \text{ Tg CH}_4\cdot\text{y}^{-1}$), according to the Global Methane Budget 2000–2017 (Saunois et al., 2020). In contrast to CO₂, the ocean is presently thought to play a minor role in the CH₄ budget (1–3 %; Saunois et al., 2020). The main tropospheric sink of CH₄ is its oxidation by reaction with hydroxyl radical (OH) in the atmosphere ($518\text{--}595 \text{ Tg CH}_4\cdot\text{y}^{-1}$). Methane is also removed, to a lesser extent, by soil uptake ($30\text{--}38 \text{ Tg CH}_4\cdot\text{y}^{-1}$). The atmospheric methane levels reached 1879.2 ± 0.6 ppb (10^{-9} v/v) in 2020 (Lan et al., 2021), approximately 2.5 times greater than the value of 722 ± 25 ppb during the pre-industrial era (Etheridge et al., 1998).

Although carbon monoxide (CO) is not a significant GHG (it is a weak absorber at about 4.65 μm), it has a major role in the troposphere affecting GHG levels. It is a major sink for OH radical, which in turn controls the CH₄ sink. In particular it has been estimated that the reaction of CO is responsible for 40 % of the removal of OH, which is the main oxidant in the troposphere (Lelieveld et al., 2016). Carbon monoxide also affects O₃ production or destruction depending on NO_x levels, and contributes to CO₂ secondary production in the atmosphere. Carbon monoxide has a short lifetime in the atmosphere of about 2 months (Khalil and Rasmussen, 1990). Its main sources are the anthropogenic emissions from fossil fuel combustion ($700 \text{ Tg CO}\cdot\text{y}^{-1}$), emissions from biomass burning that include both human-ignited and naturally-ignited fires ($500 \text{ Tg CO}\cdot\text{y}^{-1}$), natural emissions from plant leaves and marine biogeochemical cycling ($220 \text{ Tg CO}\cdot\text{y}^{-1}$), and the production of CO from oxidation of CH₄ and other volatile organic compounds (VOC, $1200 \text{ Tg CO}\cdot\text{y}^{-1}$, Zheng et al., 2019). The dominant sink of CO is the oxidation by OH radicals ($2600 \text{ Tg CO}\cdot\text{y}^{-1}$), while its removal

to the soil is estimated to be a very weak sink (Potter et al., 1996). Carbon monoxide levels have been decreasing since 2000, driven by the regulations for reduction in anthropogenic emissions in the US, Europe and China, in order to combat air pollution (Zheng et al., 2019; Daskalakis et al., 2016).

Because of the impact of CO₂, CH₄ and CO on climate and air quality, these gases are regularly monitored around the globe using ground-based (flask samples, gas concentration analyzers, including cavity ring-down spectroscopy (CRDS), and Fourier-transform infrared (FTIR) spectroscopy), airborne, and satellite measurements. Their observations, combined with numerical modeling, enable reduction of uncertainties in their emission estimates, in particular in climate sensitive regions of the globe. The Mediterranean is one of the most climatically sensitive regions of the world at the interception of three continents (Europe, Asia, Africa) where air masses of anthropogenic origin, transported mainly from Europe, the Balkans and the Black Sea (Kanakidou et al., 2011), mix with biomass burning (Sciare et al., 2008), biogenic (Liakakou et al., 2009) and other natural emissions (Gerasopoulos et al., 2011) from the regions surrounding the Mediterranean Sea (Fig. 1). This mixture of pollutants reacts chemically under the fair weather conditions with a relatively high temperature, high solar radiation and low rainfall that govern the region year-around (Kanakidou et al., 2011; Lelieveld et al., 2002; Myriokefalitakis et al., 2016).

In this study we present and discuss a 20-year data series of observations of CO₂, CH₄ and CO background levels in the remote atmosphere of the Eastern Mediterranean that are performed at the monitoring station of the University of Crete at Finokalia, Lasithi, Crete, Greece. We perform a trend analysis of these data series, compare them with data from other locations in Europe as well as with the northern hemisphere (NH) mean concentrations of these GHGs derived from the National Oceanic and Atmospheric Association (NOAA) and the Integrated Carbon Observing System (ICOS) databases. Finally, using the observed seasonal mean diurnal variation of CH₄ at Finokalia, we derive a summertime mean OH radical concentration for the region.

2. Methodology

2.1. Observations

The monitoring station of the University of Crete at Finokalia ($35^{\circ}20'N$, $25^{\circ}40'E$, 250 m ASL) (Fig. 1) is representative of the regional background atmosphere since no significant anthropogenic activities occur within 15 km around the station (Mihalopoulos et al., 1997). The station is located 250 m above sea level on the coast at about 70 km North East of Heraklion city and is facing the sea within the sector of 270° to 90° . Air samples are collected from the top of a 12-m mast. During summer the station is affected by northerly and north-westerly winds (Central Europe and the Balkans), while the remaining period and particularly during spring and fall it is strongly impacted by southern and south-western air masses originating from North Africa in addition to the prevailing north-westerly winds (Mihalopoulos et al., 1997).

CO₂, CO and CH₄ concentration observations began at Finokalia in 2002, first with flask sampling then with a Cavity Ring Down Spectrometer (PICARRO G2401) installed in June 2014 for continuous measurements; while flask sampling continued on a sporadic basis for comparison with the on-line analyzer measurements. The two datasets compare well as shown in Fig. S1.

Pairs of flasks were sampled weekly with a sampling unit consisting of a pump drawing air through a chemical drying cartridge. Air was collected in 1 L glass flasks, pressurized to 2 bar absolute pressure. Flasks were analyzed at Laboratoire des Sciences du Climat et de l'Environnement (LSCE) on a commercial gas chromatograph (GC), 6890 N from Agilent Technologies, which was adapted for flask measurements (Lopez et al., 2012; Schmidt et al., 2014; Lopez et al., 2015). The GC was equipped with a flame ionization detector for CH₄ and CO₂. A reduction gas detector from Peak Performer was coupled to the GC for CO measurements. The instrument was regularly calibrated against two standards and a known target gas was

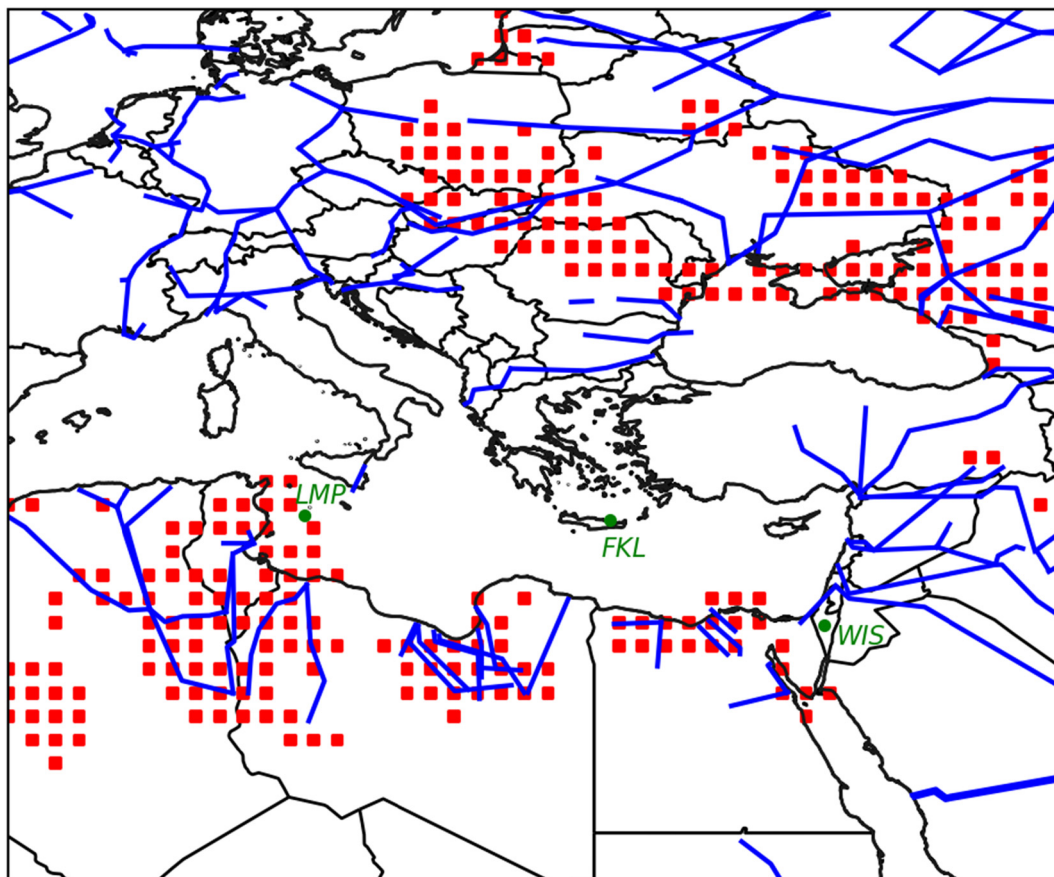


Fig. 1. Finokalia (FKL), Lampedusa (LMP) and Weizmann Institute of Science (WIS) atmospheric monitoring stations in the Mediterranean (green circles) and the location of oil pipelines (blue lines) and oil refineries (red squares) as derived from the Harvard database (data from <https://hgl.harvard.edu/catalog/>, last access on 12 April 2022). (For interpretation of the references to color in this figure legend, the reader is referred to the web version of this article.)

injected every 30 min, showing a short-term repeatability of approximately 0.1 ppm CO₂, 1 ppb CH₄, and 2 ppb CO.

Continuous measurements, performed via the CRDS analyzer, were setup to follow the ICOS specifications (ICOS RI, 2020; Yver-Kwok et al., 2021). A set of four calibration cylinders, a short-term target and a long-term target are calibrated and provided by LSCE for the calibration at Finokalia. All data (flask and continuous) presented in this study are calibrated against the World Meteorological Organization (WMO) scales: WMOX2019 for CO₂, WMO X2004A for CH₄ and WMO CO X2014A for CO.

Aggregating the data over time is the final step in the process. For in situ data, the 1 min, hourly and daily means are computed. All the means are calculated using data from the nearest temporal aggregation level rather than the raw data, as recommended by the World Data Centre for Greenhouse Gases (WDCGG). This means that raw data are utilized to compute one-minute averages, which are subsequently used to compute hourly averages and so on (Hazan et al., 2016). For the present study, we calculated and analyzed the monthly and daily mean values.

2.2. Data analysis

In order to analyze the variabilities in the observed concentrations, at different time scales, two different methodologies have been used. First, we used the methodology of the seasonal-trend decomposition procedure (STL), based on LOcally Estimated Scatter plots Smoothing (LOESS) using locally weighted regression, developed by Cleveland et al. (1990). LOESS regression is a nonparametric technique that instead of creating a global model for the whole function space, like linear regression, it creates a local model for each point of interest based on data from nearby the query point. For this aim, each data point is transformed into a weighting

factor that indicates the data point's effect on the forecast. In general, data points that are near the current query point are given more weight than data points that are far away. LOESS curves can indicate data trends and seasonal cycles that are difficult to model using a parametric curve. This method decomposes the time series into the trendline (Fig. S2), the seasonality (Fig. S3), and the residual (Fig. S4), assuming that the timeseries are additive i.e., that each observation in the series can be expressed as a sum of the components. A python program available on the web has been used for these calculations (<https://www.statsmodels.org/devel/generated/statsmodels.tsa.seasonal.STL.html>, last access 6 May 2022). The only obstacle for this method is that the program does not work with data having large gaps, so this method was applied only to the PICARRO continuous data.

For that reason, we have also developed another simple method of seasonal trend decomposition based on linear regression (STLR) that has been applied to the combined dataset of flask and continuous observations. We first apply a linear regression to the monthly mean observations for all the years to calculate the intercept and the slope from our data. We then calculate the residual, i.e. the distance of each monthly mean value from the linear regression line, by subtracting from the original data the value reconstructed using the linear regression. These monthly residuals are used to calculate the mean residual for each month averaged over the years of the studied period. This mean residual value for each month is then subtracted from the respective month of each year leading to the deseasonalized timeseries. Both STL and STLR methods have been successfully evaluated (Fig. S5) by applying them to the NOAA flask measurements and comparing the deseasonalized CO₂ monthly mean values with those reported for Mauna Loa on NOAA's website (https://gml.noaa.gov/webdata/ccgg/trends/co2/co2_mm_mlo.txt, last access on 01 April 2022).

Seasonal variations have been investigated by using both the STL seasonal component (Fig. S3) and the monthly mean concentrations normalized to the mean of the observed concentrations of the respective year. Diurnal variations have been calculated by normalizing the hourly concentrations to the mean daily value of the respective day. Monthly and then seasonal mean diurnal variations are derived.

The observations at Finokalia are also compared with publicly available data for CO₂, CO and CH₄ from monitoring stations of the Integrated Carbon Observing System (ICOS) network in Europe (<https://www.icos-cp.eu/data-products/atmosphere-release>, last access on 08 April 2022) and from the NH stations of the National Oceanic and Atmospheric Association (NOAA) database (<https://gml.noaa.gov/dv/data/>, last access on 8 April 2022), in particular with data from Lampedusa, a nearby station in the Central Mediterranean, as well as CH₄ and CO level 2 data from the TROPOMI Sentinel 5P instrument using the WFM-DOAS v1.5 product (https://www.iup.uni-bremen.de/carbon_ghg/products/tropomi_wfmd/index.php, last access on 8 April 2022) (Schneising et al., 2019). TROPOMI Sentinel-5P was launched in October 2017, with data available from December 2017. It has a sun-synchronous orbit at an altitude of approximately 824 km and a swath size of 2600 km. It has a 16-day orbital cycle reaching Equator at 13:30 local time. TROPOMI is a nadir-viewing spectrometer with channels in the ultraviolet spectral region in the NIR and SWIR. The spatial resolution of both CO and CH₄ data products was 7.0 × 7.0 km at the beginning of the mission in 2017 and 7.0 × 5.5 km since 6 August 2019. For our study we used daily TROPOMI data from 2018 to 2020 to calculate the monthly values for a grid box with a radius of 100 km centered at the Finokalia station. In addition, the Finokalia observations have been compared to the surface observations of GHG by CRDS using the urban background site of Thission in Athens by Dimitriou et al. (2021) as well as to the column observations by FTIR at the Aristotle University of Thessaloniki in Thessaloniki by Mermigkas et al. (2021) for the period 2019–2020.

3. Results and discussion

We analyzed the concentrations of GHG measured at Finokalia station, both based on the flasks and on the continuous measurements. The continuous data are first averaged per hour, and these values are then here used for analysis.

3.1. Interannual trends since 2002

Fig. 2 shows the interannual variability of CO₂, CH₄ and CO over the 20 years of observations combining the discontinuously collected flask samples (2002–2014; blue) with the monthly mean of the continuous observations since June 2014 (green). Interannual changes are the net result of the emissions (natural climate-driven and anthropogenic) and those of the sinks (physical, biological or chemical), which can be modulated by interannual variation of the atmospheric circulation. An overall increasing trend is observed for both CO₂ and CH₄ with annual mean concentrations (\pm standard deviation) spanning from 375.2 \pm 3.1 ppm and 1862.0 \pm 4.0 ppb in 2002 to 417.0 \pm 4.4 ppm and 1978.2 \pm 9.9 ppb in 2021, respectively.

These values are close to those observed in Lampedusa in the Central Mediterranean to the west of Crete (see Fig. S6 and discussion in Section 3.2) and lower than the respective levels observed at the urban background station of Thission in the large agglomeration of Athens, mainland Greece, to the northwest of Finokalia. Indeed, in 2019 monthly mean CH₄ concentrations at Thission exceeded those at Finokalia by approximately 40 ppb, depending on month compared (Dimitriou et al., 2021). For CO₂ this difference between the urban background station and the Finokalia regional background station is the highest during winter months, when it reaches about 30 ppm (Dimitriou et al., 2021). An interannual trend opposite to that of CH₄ and CO₂ is observed for CO at Finokalia and shows a clear decrease from 171.6 \pm 8.0 ppb in 2002 to 120.3 \pm 12.6 in 2021. This trend reflects the effectiveness of the legislation for the improvement of air quality (Lamarque et al., 2013) as well as the potential change in

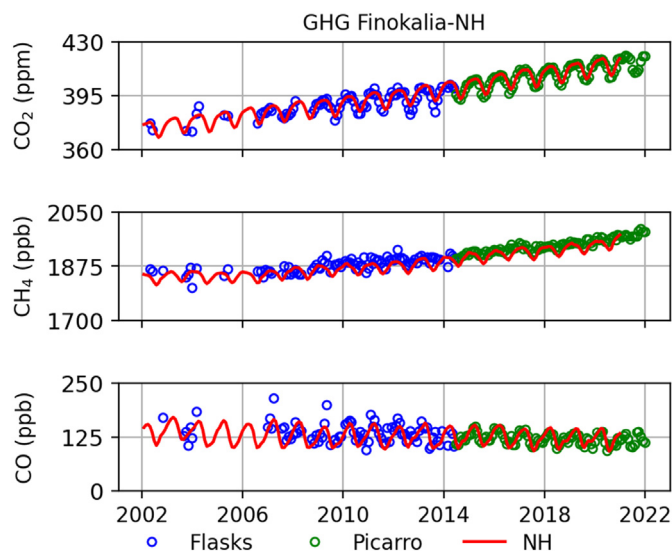


Fig. 2. Observations of CO₂ (top), CH₄ (middle) and CO (bottom) at the Finokalia atmospheric monitoring station, Lasithi, Crete. Green circles depict monthly mean data based on hourly PICARRO continuous measurements (since June 2014), blue circles are monthly means from flask observations, the red line depicts the monthly mean observations in the north hemisphere based on available NOAA flask observations (see text). (For interpretation of the references to color in this figure legend, the reader is referred to the web version of this article.)

the tropospheric oxidants, in particular the OH radical that is the main oxidant reacting with CO. Note that the CO levels from flask observations in 2002 agree with the observations in the area during the MINOS campaign in 2001 reported by Lelieveld et al. (2002), who estimated the contribution from western and eastern Europe to boundary layer CO in the Eastern Mediterranean at about 60–80 %, mainly from fossil fuel use. These data are also in line with the observations of 170 \pm 27 ppb observed at the forest of Pertouli in the north of Greece in 1997 (Gros et al., 2002). This CO background concentration is mainly controlled by long-range transport of polluted air masses to the region, as shown by Myriokefalitakis et al. (2016) who also estimated the annual mean contribution of regional anthropogenic sources of CO at approximately 20 %.

Because the data show clear seasonal patterns that will be further discussed in Section 3.2, the STL and STLR programs (see Section 2.2) have been applied to deseasonalize them in order to deduce the long-term trends and interannual variations for each of the studied compounds (Figs. S2–S4). Trends were calculated for the whole period, including the flask period, with larger uncertainties for this earlier period. However, the flask observations and PICARRO data compare rather well as shown in Fig. S1 for CO₂ over the period 2014 to 2018, when both type of observations are available. Thus, we discuss the results for different periods but we focus mainly on the recent period with continuous measurements that provide a more accurate picture of the variability of the studied compounds due to the larger number of observations (about 720 datapoints/month) than the flask data. Nevertheless, despite the scarcity of the data, the flask observations of the three measured species from the earlier years (2002–2014) follow similar interannual trends. The derived clearly increasing trends for CO₂ are 2.4 ppm·y⁻¹ (since 2002, all data) and 2.5 ppm·y⁻¹ (since 2014, PICARRO data). For CH₄ the entire dataset shows a 7.5 ppb·y⁻¹ increase over the 20 year period while the PICARRO data (since 2014) indicate an accelerated increase since 2018 (an increasing rate of 12.4 ppb·y⁻¹). In contrast, a decreasing trend of CO has been found for the 20 year period (all data) corresponding to 1.6 ppb·y⁻¹, similar to the trend derived for the period 2014–2021 (PICARRO data). The trend in CO is the result of a strong decrease until 2017 (2.5 ppb·y⁻¹) followed by a small increase the last 3 years (0.2 ppb·y⁻¹).

It is interesting to compare these results with the NH patterns of the studied compounds as recorded by the NOAA network. As expected, due

to its long lifetime and the remote location of the background station at Finokalia, CO₂ follows the observed NH mean concentration changes (Fig. 2, top, continuous red line). In contrast, CH₄ observed concentrations at Finokalia are approximately 13.2 ± 10.9 ppb higher than the mean NH values for the 20-year record and 13.0 ± 5.6 ppb for the last 7-year period (Fig. 2-middle, continuous red line, and supplementary Figs. S7, S8). Considering the high photochemical activity in the region (Berresheim et al., 2003; Lelieveld et al., 2002) the higher than NH average levels of CH₄ are likely to be due to the vicinity of important regional sources of CH₄ from oil and natural gas exploitation (extraction, storage and transportation activities, <https://hgl.harvard.edu/catalog/>, Fig. 1) or other local sources, like livestock farming, that lead to an increase in the background CH₄ levels. This is supported by the comparison with observations from Lampedusa in the Central Mediterranean, the only other nearby station in the Mediterranean with long GHG observations, that shows slightly lower CH₄ levels (by 11.0 ± 6.9 ppb) as well as a smaller increasing trend (by $0.4 \text{ ppb} \cdot \text{y}^{-1}$) than at Finokalia (Figs. S6, S8). However, at the eastern edge of the Mediterranean, the Weizmann station in Israel (Fig. S8) shows CH₄ levels and trends comparable to Finokalia, indicating that the higher than the NH average CH₄ levels and the faster increase is a regional than a local characteristic.

Carbon monoxide levels at Finokalia appear to be on average slightly higher than the NH average, by 2.6 ± 13.6 ppb, when considering the 20-year record, and slightly lower, by 2.7 ± 6.9 ppb, when considering the last 7 years (Fig. 2 and Fig. S7). These differences are not significant when accounting for the variability in the observations. In addition, comparing the PICARRO data at Finokalia to the Lampedusa observations (2014–2020), CO concentrations at Finokalia appear to be lower by 1.8 ± 8.5 ppb (Fig. S6), while their decreasing trend is higher by about $2 \text{ ppb} \cdot \text{y}^{-1}$. Although these concentration differences are not significant, they could reflect the high photochemical activity, and therefore the high OH sink of CO in the region. This could be overcoming any increase of the secondary source of CO by CH₄ and oxidation of other volatile organic compounds (VOC) in the region, and corroborates with the reduction in CO primary sources due to legislation. Furthermore, compared to the NH mean, similar seasonal behavior of CO concentrations is found, with the exception of the peaks that appear during the summer months, which can be attributed to regional biomass burning emissions. Indeed, it is interesting to mention that the decline in ambient CO concentrations is a global trend resulting from policy implementation for the improvement of air quality (Lowry et al., 2016). In line with the global trend, in Greece during and after the economic crisis in 2009–2010, CO, nitrogen oxides and nonmethane volatile organic compounds emissions are considerably decreasing. This reduction happens despite the increase of the population of circulating vehicles, as there is a marked increase in less polluting vehicles ((European Environment Agency, 2021), Greece 2021: National inventory report, <https://unfccc.int/ghg-inventories-annex-i-parties/2021>; last access Nov. 27, 2022). CO emission reduction is reflected in CO levels at Finokalia that are mainly affected by long-range transported pollution (Myriokefalitakis et al., 2016).

3.2. Seasonal variability

Based on the continuous hourly observations since June 2014, CO₂ monthly mean concentrations range from 396.3 ± 3.6 ppm in June 2014 to 420.7 ± 2.2 ppm in December 2021, with the lowest concentration in Aug. 2014 (392.9 ± 2.2 ppm) and the highest in March 2021 (421.4 ± 0.5 ppm). Fig. 3a depicts the seasonal variability of the studied species as derived from the 20 years of observational data (squares) and from the continuous observations since 2014 (circles), using monthly mean observations normalized to the annual mean of the respective year. Both the 20 year and the last 7 years datasets show similar patterns. We will further discuss the more representative last 7 years of data (2015–2021, circles). CO₂ (Fig. 3a) shows maximum values from November to April and the lowest values are in July and August with a seasonal amplitude of about 2.9 %

(derived by subtracting the minimum from the maximum normalized monthly mean values in Fig. 3a). This behavior can be explained by the dependence of CO₂ on the photosynthesis of plants (Allard et al., 2008; Walker et al., 2021). This maximizes under intensive photochemistry conditions which dominate in the region during late spring, summer and early autumn (Kanakidou et al., 2011). Vegetation in the northern hemisphere flourishes during spring and summer, resulting in increased photosynthesis and consequently a decrease of atmospheric CO₂ that is captured by the biosphere. Fig. S9 compares CO₂ seasonal variability at Finokalia with that of other stations in Europe. As expected, due to the relatively remote location of Finokalia compared to the other ICOS stations where most of them are in continental Europe and thus are strongly affected by vegetation, the coastal site of Finokalia on the island of Crete shows a smaller seasonal magnitude than at the ICOS stations as a whole. Concentrations of CO₂ at Finokalia show similar seasonality and seasonal amplitude to the Lampedusa (Central Mediterranean) and Weizmann (Israel) stations (Fig. 3b). Carbon dioxide concentrations at Finokalia decrease faster than at the two other sites from spring to summer, followed by a slower increase towards winter, indicating a more efficient regional sink and/or weaker regional sources than at the other sites.

Monthly mean values of CH₄ calculated from the daily observations, range from 1900.8 ± 24.6 ppb (10^{-9} v/v) in June 2014 to 1987.9 ± 15.3 ppb in Dec. 2021 with the lowest monthly mean concentration in July 2014 (1899.4 ± 15.2 ppb) and the highest in Oct. 2021 (1997.9 ± 14.5 ppb). At Finokalia CH₄ concentrations do not depict a clear seasonal variation, as the factors affecting it are multiple. Atmospheric transport, primary emissions of anthropogenic and natural origin and secondary chemical destruction of CH₄ from OH radicals in the troposphere are the main factors affecting CH₄ concentrations and seasonality (Khalil and Rasmussen, 1983; Rigby et al., 2017). However, a seasonal amplitude of about 1.1 % is derived from the normalized monthly mean concentrations (Fig. 3c). High values are observed from August to March and the lowest in June and July (Fig. 3c). These low values can be explained by the chemical consumption of methane by the OH radical, the concentrations of which maximize during spring and summer due to the intense sunlight and the high O₃ levels (Berresheim et al., 2003; Gerasopoulos et al., 2005). In Fig. 3d and supplementary Fig. S9 the continuous observations at Finokalia station are compared with monthly mean values from ICOS stations in Europe and with data from Lampedusa and Weizmann stations from the NOAA network. Due to the long lifetime of CH₄ (about 10 years, (Saunois et al., 2020)) its hemispheric mean seasonality is not expected to be affected by regional sources or sinks. Finokalia data show a much smaller seasonal amplitude than the ICOS data (Fig. S9). However, they agree reasonably well with those at the Weizmann station, with a minimum in June and high values in winter (Fig. 3d). Lampedusa station in the Central Mediterranean shows a more pronounced seasonality with the minimum in July delayed by one month compared to Finokalia and Weizmann observations.

CO hourly concentrations at Finokalia range from about 70 to 436 ppb over the entire studied period, with the highest values observed in August 2021 when intensive fires occurred over Greece and Turkey affecting the entire Eastern Mediterranean. Based on the continuous hourly observations from the last 7 years, monthly mean CO concentrations vary from 150.5 ± 23.5 ppb in March 2015 to 93.8 ± 6.6 ppb in June 2020 (Fig. 3e). Overall CO at Finokalia shows a late winter/early spring (Jan–April) maximum, which is affected by the agricultural burnings all over the island of Crete. It also reflects a net photochemical gain for CO resulting from oxidation of high concentrations of volatile organics during spring, under conditions of significant photochemical activity. CO shows a summer (June) minimum when its photochemical destruction by reaction with the OH radical maximizes. Overall, the seasonal cycle of CO, with an amplitude of 28 %, reflects the combined effect of the seasonal variation of the primary and secondary emissions and of the photochemical sink by reaction with the OH radical. However, a secondary smaller seasonal maximum is also seen in CO monthly mean concentrations associated with summer time open fire emissions in the Mediterranean that are both naturally and human-induced.

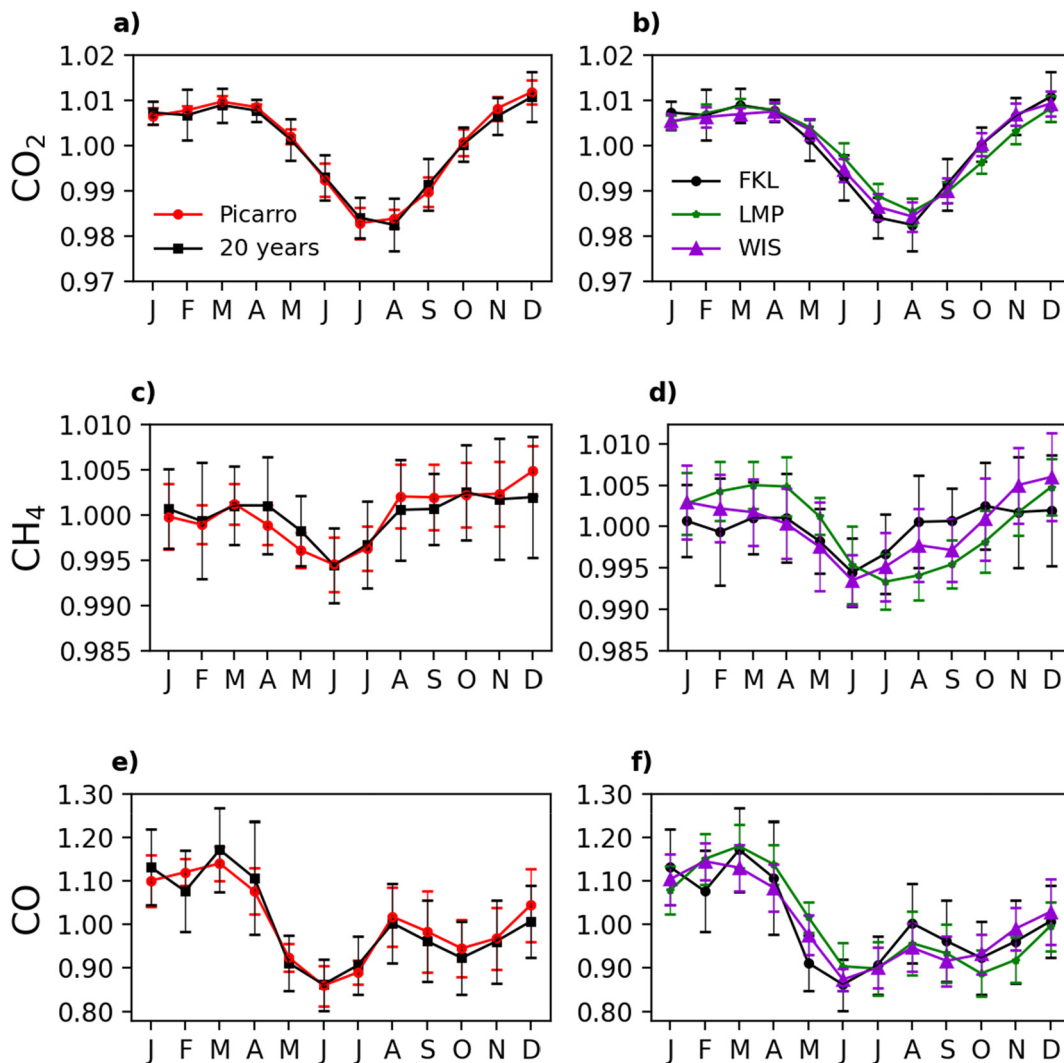


Fig. 3. Normalized monthly mean variability of CO₂ (a), CH₄ (c) and CO (e) at Finokalia (FKL) atmospheric monitoring station as derived from continuous observations (red symbols and line; June 2014–Dec 2021) and from all data (20 years). Comparison of normalized FKL mean seasonality (20 years) with those observed (flask measurements) at Lampedusa (LMP; from 2006 to 2020) and Weizmann (WIS; from 2002 to 2020) stations in the region (b, d, f) (see also Fig. S7). (For interpretation of the references to color in this figure legend, the reader is referred to the web version of this article.)

This secondary maximum is also seen in the data from the Lampedusa and Weizmann stations (Fig. 3f); while it clearly differentiates the seasonal patterns of these stations from the overall ICOS European network seasonality (Fig. S9). Unlike CO₂ and CH₄, which as earlier discussed have long lifetimes in the atmosphere, CO has a much shorter lifetime (about 2 months depending on the atmospheric conditions (Khalil and Rasmussen, 1990)) and therefore responds faster than the other two GHGs to its emission changes.

Fig. 4a and b compares the normalized near-surface monthly mean variation of CH₄ and CO respectively, as derived from the in-situ observations at Finokalia, with the normalized total columns derived from TROPOMI satellite observations and from FTIR measurements at Thessaloniki for the period 2019–2020, when both in-situ and satellite observations are available (see Section 2). Since satellite and FTIR observations measure the total column, differences with the surface-derived seasonality are to be expected. Interestingly, satellite-derived total column CH₄ levels at Finokalia show a similar pattern to the FTIR normalized column observations at Thessaloniki with a low in February and March. However, the in-situ near-surface observations at Finokalia indicate values very close to the annual mean during that period, most probably associated with near-surface CH₄ pollution, e.g. from sheep and goats on the island of Crete or

oil and natural gas exploration and exploitation in the vicinity, and the different air masses above. On the other hand, TROPOMI seasonal variability for total column CO is in general agreement with the in-situ near-surface observations at Finokalia and with FTIR column observations at Thessaloniki. It shows an April maximum (Fig. 4b), which is not so marked when accounting for the satellite observations variability, expressed by the standard deviation of the overpasses within each month. It also reflects the secondary late summer high CO values attributed to biomass burning emissions affecting the region during that period. Furthermore, CO column seasonal variability derived from the satellite observations presents its lowest values late autumn (Oct., Nov.), while near surface CO concentration variability shows minima in June and July. However, when accounting for the variability (standard deviation) within each month, these differences between the near-surface and the total column seasonality are not significant. The general good agreement between the seasonal variability of in-situ near-surface CO and satellite-derived column CO shows the large contribution of near-surface CO to the total CO column. It also shows that since TROPOMI CO column observations are coherent with the in-situ near-surface observations, TROPOMI provides invaluable data to construct the global distribution of CO in the troposphere, in particular covering regions where in-situ observations do not exist.

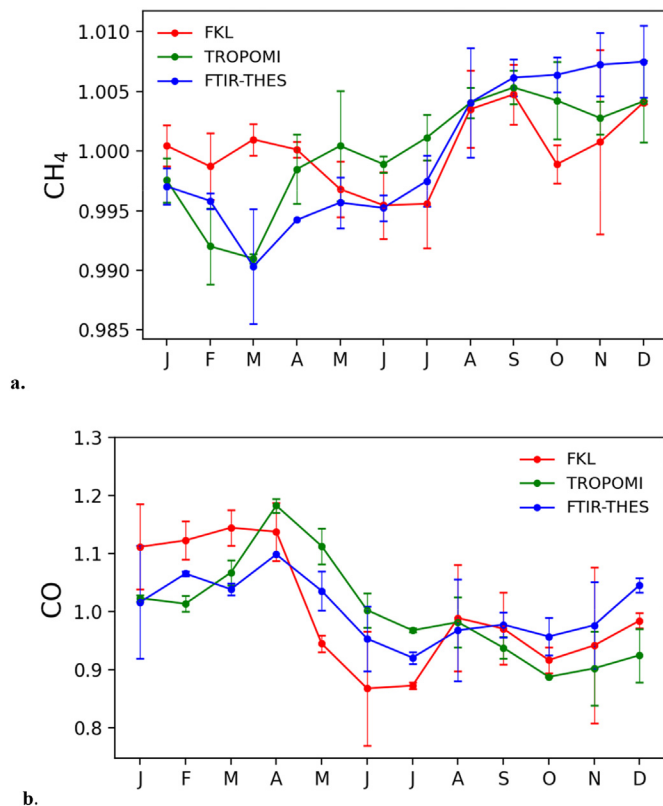


Fig. 4. Monthly mean variability (and standard deviation) of normalized levels of CH₄ (a) and CO (b) as derived from the in situ near-surface observations at Finokalia (red line) and from TROPOMI total column observations with a colocation radius of 100 km (green line). For CH₄ comparison is also done with FTIR measurements at Thessaloniki (see text). Comparison is done for the years 2019–2020. (For interpretation of the references to color in this figure legend, the reader is referred to the web version of this article.)

3.3. Diurnal variability

In the following, the diurnal variability of the studied compounds is investigated on a seasonal basis (winter: December January February, DJF, spring: March April May, MAM, summer: June July August, JJA, autumn: September October November, SON) using the hourly data available since June 2014. For this, first hourly concentrations have been normalized to the mean daily value of the respective day and then monthly and thereby seasonal averages have been calculated for each hour.

A small diurnal variation of CO₂ is observed only in winter and spring with diurnal amplitudes of about 0.25 % and 0.28 %, respectively (supplementary Fig. S10). This variation that appears to follow solar illumination is probably due to photosynthesis during daytime, which is more intense during the growing period. It is worth noting that during winter the area has significant growth and greening of the vegetation, while in the summer the region is very dry causing a browning and significant reduction in vegetation growth and photosynthesis. In addition, in summer and autumn, the hourly variability (shown by the standard deviation) is too high, prohibiting the observation of any significant diurnal variation.

Apart from winter, when CH₄ does not show any significant diurnal variation, during the other seasons a mid-day minimum is observed in the overall weak CH₄ diurnal variability (supplementary Fig. S11). The strongest diurnal variability appears mainly during summer (diurnal amplitude of about 0.24 %, Fig. 5a) followed by spring's variability (diurnal amplitude of about 0.16 %). This can be partially attributed to the CH₄ daytime sink from reaction with the OH radical. This radical presents its highest concentrations during late spring and summer because of the intense solar radiation in the region. Maximum values of CH₄ are observed in the early

morning and evening hours due to the absence of the sunlight and weak air circulation (Gerasopoulos et al., 2006).

The strongest diurnal variability of CO is observed in summer (Fig. 5b) and winter (diurnal amplitude of about 1.4 % and 2.3 %, respectively, supplementary Fig. S12). Summer CO variability is driven by both sources and sinks. The high summertime concentrations of OH radicals result both in high CO loss by chemical reaction with OH to produce CO₂ and in high CO production during the atmospheric oxidation of VOC, including CH₄; these two impacts having opposite effects on CO concentration. In addition, fires that often occur in the Mediterranean during summer further increase CO sources. Winter-time variability shows CO minimum values early in the morning, most probably reflecting the opening of the boundary layer. Here the surface air rich in CO, due to the burning of wood/olive tree branches during agricultural activities, is diluted by mixing with cleaner free tropospheric air.

3.4. Hydroxyl radicals

From the summer averaged diurnal variation of CH₄ and CO (Fig. 5a, b) we calculated the mean OH radical concentrations that can explain the observed morning to mid-day reduction in CH₄ and CO concentrations in summer over the period 2014–2021. Such an approach neglects any dilution due to the mixing of surface air with free tropospheric air, or surface deposition, and assumes oxidation by the OH radical as the only reason for the morning to mid-day decrease in the concentrations of these reactive species. In addition, for CO it neglects the photochemical production of CO during the day through the oxidation of CH₄ and other VOC that can be a significant source of CO on a regional scale. Therefore, only an approximate estimate of seasonal day-time mean OH radical concentration can be derived here from CH₄ and CO seasonally averaged diurnal variability. For this we consider the first order decay of these compounds by reaction with the OH radical following the Eq. (1):

$$\frac{\Delta C}{C_0} = e^{-k_{OH}OHt} \quad (1)$$

where C_0 is the initial/early morning normalized concentration, ΔC is the difference between the normalized values of the early morning (6 am local time) and mid-day (2 pm local time) values, k_{OH} is the rate constant for the reaction of the OH radical with CH₄ and CO, respectively that is calculated using the mean temperature and pressure of each season for the respective year ($k_{OH,CH_4} = 1.85 \times 10^{-12} \exp(-1690/T)$; $k_{OH,CO} = 1.44 \times 10^{-13} (1 + [N_2]) / (4.2 \times 10^{19} \text{ molecule}\cdot\text{cm}^{-3})$) (Atkinson et al., 2006), OH is the mean concentration of the OH radical, and t is the time period over which the decay is observed (in s).

The results are depicted in Fig. 5c for CH₄ and indicate a mean OH concentration during daylight of $1.5 (\pm 0.3) 10^7 \text{ molecules}\cdot\text{cm}^{-3}$ over the 8 summers from 2014 to 2021, ranging between approximately $1.1 \times 10^7 \text{ molecules}\cdot\text{cm}^{-3}$ (in 2014 and 2021) and $2.1 \times 10^7 \text{ molecules}\cdot\text{cm}^{-3}$ (in 2015). This corresponds to $0.7 (\pm 0.2) 10^7 \text{ molecules}\cdot\text{cm}^{-3}$ of OH averaged over 24-h over the 8 summers period. The mean daytime OH concentration derived from the observed decrease of CO from the morning to noon in summer is almost 4.5 times lower (at $3.1 \times 10^6 \text{ molecules}\cdot\text{cm}^{-3}$) and this difference can be explained by the unaccounted regional production of CO from VOC oxidation. Indeed, considering that the observed CH₄ daytime decrease (Fig. 5a) ultimately leads to CO formation that is also depleted by the OH radical during daytime, roughly a factor of 4.5 times higher OH radical concentration (i.e., $1 \times 10^7 \text{ molecules}\cdot\text{cm}^{-3}$) would be needed to explain the observed CO concentration changes than the above-derived value based on the observed CO diurnal variability, assuming no photochemical sources for CO. Overall, the thus deduced 24-h mean OH value of $0.7 (\pm 0.2) 10^7 \text{ molecules}\cdot\text{cm}^{-3}$, is in general agreement with the respective mean OH levels of $4.5 (\pm 1.1) 10^6 \text{ molecules}\cdot\text{cm}^{-3}$ observed by Berresheim et al. (2003) at Finokalia during summer 2001; the only existing OH observations at Finokalia.

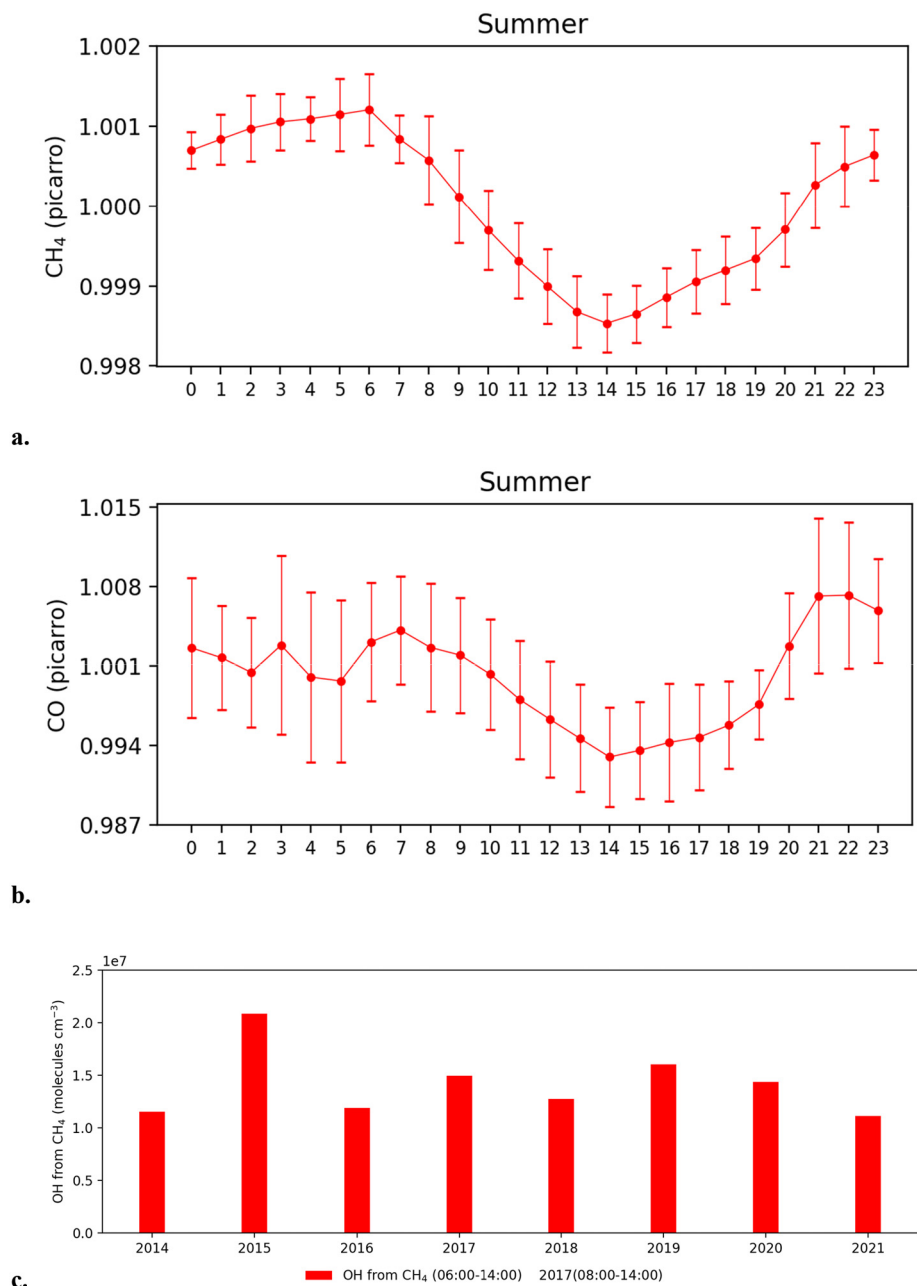


Fig. 5. a. Average summertime diurnal variation of CH₄ for the period 2014–2021; b Average summertime diurnal variation of CO for the period 2014–2021; c. interannual variability of summertime average OH radical concentrations as derived from the summertime average diurnal variability of CH₄ between 06:00 and 14:00 local time for all years except 2017 when the period 08:00–14:00 is used following the observed diurnal pattern (see text).

It is worth noting that in Fig. 5c for 2017 the OH concentrations are derived from the summer mean CH₄ decrease between 08:00 and 14:00 since that year CH₄ shows a different diurnal pattern than the other years of our study with morning maximum at 08:00 rather than at 06:00. Interestingly, CH₄ concentrations show a discontinuity in the increasing trend in 2016 (supplementary Fig. S8), increasing faster than in earlier years, and a decreasing trend during the first half of 2017. It is remarkable that 2016 was an El Nino year and the warmest year of the century following a relatively cooler year in 2015. Such a pattern is also seen in the record of the Weizmann station, although the peak in CH₄ concentration in 2016 is reached a few months earlier than at Finokalia. Furthermore, the Weizmann station also experienced the fastest increasing CH₄ trend over 2014–2020, which is the common period of observations with Finokalia. This 2016/2017 peak/anomaly is also seen at Lampedusa as well as in

the mean of the NH record, where it coincides with the Finokalia peak but shows lower CH₄ concentrations.

4. Conclusions

In the present study a 20-year-long observational data series of the two major greenhouse gases, CO₂ and CH₄, as well as CO from the Finokalia atmospheric observatory on the island of Crete in the Eastern Mediterranean are presented. These data consist of the longest record of GHG in the atmosphere for the Eastern Mediterranean and are analyzed with regard to their interannual, seasonal and diurnal variability. Monthly mean CO₂ levels at Finokalia reached 421.4 ppm in March 2021. Hourly CH₄ levels at Finokalia ranged from 1805 to 2041 ppb with an average value of 1900.2 ± 39.6 ppb for the period 2002–2021. Hourly CO levels ranged from 47

to 436 ppb with an average value of 133.7 ± 18.1 ppb for 2002–2021. The observed increasing trends for CO_2 of $2.4 \text{ ppm}\cdot\text{y}^{-1}$ since 2002 and for CH_4 of 7.5 ppby^{-1} (20-year data since 2002) and 12.4 ppby^{-1} (2018–2021) agree with those derived from the NOAA network for NH and reflect the increase in anthropogenic emissions. However, CH_4 concentrations at Finokalia are higher than the NH mean observations, indicating the impact of significant regional sources of this GHG. Future studies with isotopic measurements could help identify the origin of these regional sources. The observed seasonal variability at Finokalia, with high CO_2 and CH_4 values during winter and low during summer, is in line with those derived from the ICOS network over Europe but weaker in amplitude, reflecting the background conditions of this coastal station in the Eastern Mediterranean. CO_2 seasonal variation shows the dependence of CO_2 on photosynthesis of plants with maximum CO_2 concentrations in winter and autumn and minimum values in summer, reflecting wood burning for heating or agricultural activities in winter and photosynthesis in spring. Small diurnal variability in CO_2 was observed only in winter and in spring reflecting emissions and photosynthesis variability respectively. The observed small seasonal variability of CH_4 , with peak values in winter and minimum values in summer, is probably due to the methane consumption by OH radicals that are present in higher concentrations during the summer months. Indeed, the highest significant diurnal variability of CH_4 was observed in the summer months, with peak values in the early morning and evening hours and minimum values around 14:00 local time. CO shows a decreasing trend of 1.6 ppby^{-1} since 2002 and a seasonality with a primary maximum in late winter/early spring, a minimum in June and a secondary maximum in August; the latter is most probably associated with open fires in the region. The interannual decrease of CO appears to be related mainly to the continuous reduction in emissions from anthropogenic sources and is also influenced by changes in OH radical concentrations that affect both CO secondary photochemical sources and sinks.

The daytime mean seasonal decrease of CH_4 and CO agrees with their loss by reaction with 24-h mean OH radicals, which is of the order of $0.7 \pm 0.2 \times 10^7 \text{ molecules}\cdot\text{cm}^{-3}$ over the region during the summer. The data presented here from the Finokalia station provide an ideal reference of the atmospheric background for investigating the contribution that cities make to GHG levels (see for instance in Dimitriou et al., 2021). They are also used together with satellite observations in ongoing inverse modeling exercises to improve the accuracy of countries' emission estimates in the extended region.

CRedit authorship contribution statement

NG collected and statistically analyzed the data, wrote the initial manuscript, NK and GK supported the measurements at Finokalia station, MR contributed to the quality control of the data, ND contributed to the satellite data analysis, MM provided the FTIR data from Thessaloniki station. MK, NM and MR conceived the study, MK supervised the work and contributed to the manuscript writing, all authors contributed to data interpretation and commented on the manuscript.

Data availability

Data will be made available on request.

Declaration of competing interest

The authors declare that they have no known competing financial interests or personal relationships that could have appeared to influence the work reported in this paper.

Acknowledgements

We acknowledge support of this work by the project SNO ICOS-France-Atmosphere and by the Action "National Network on Climate Change and its Impacts (CLIMPACT)" implemented under the project "Infrastructure

of national research networks in the fields of Precision Medicine, Quantum Technology and Climate Change", funded by the Public Investment Program of Greece, Greek General Secretary of Research and Technology/Ministry of Development and Investments. ND, MK acknowledge support by the Deutsche Forschungsgemeinschaft (DFG, German Research Foundation) under Germany's Excellence Strategy (University Allowance, EXC 2077, University of Bremen). We thank Oliver Schneising for useful comments on the manuscript and for providing the TROPOMI product of IUP.

Appendix A. Supplementary data

Supplementary data to this article can be found online at <https://doi.org/10.1016/j.scitotenv.2022.161003>.

References

- Allard, V., Ourcival, J.M., Rambal, S., Joffre, R., Rocheteau, A., 2008. Seasonal and annual variation of carbon exchange in an evergreen Mediterranean forest in southern France. *Glob. Chang. Biol.* 14 (4), 714–725. <https://doi.org/10.1111/j.1365-2486.2008.01539.x>.
- Atkinson, R., Baulch, D.L., Cox, R.A., Crowley, J.N., Hampson, R.F., Hynes, R.G., Jenkin, M.E., Rossi, M.J., Troe, J., 2006. Evaluated kinetic and photochemical data for atmospheric chemistry: volume II - gas phase reactions of organic species. *Atmos. Chem. Phys.* 6 (11). <https://doi.org/10.5194/acp-6-3625-2006>.
- Berresheim, H., Plass-Dülmer, C., Elste, T., Mihalopoulos, N., Rohrer, F., 2003. OH in the coastal boundary layer of Crete during MINOS: measurements and relationship with ozone photolysis. *Atmos. Chem. Phys.* 3 (3), 639–649. <https://doi.org/10.5194/acp-3-639-2003>.
- Cleveland, R.B., Cleveland, W.S., Terpenning, I., 1990. STL: a seasonal-trend decomposition procedure based on loess. *J. Off. Stat.* 6 (1), 3.
- Daskalakis, N., Tsigaridis, K., Myriokefalitakis, S., Fanourgakis, G.S., Kanakidou, M., 2016. Large gain in air quality compared to an alternative anthropogenic emissions scenario. *Atmos. Chem. Phys.* 16 (15), 9771–9784. <https://doi.org/10.5194/acp-16-9771-2016>.
- Dimitriou, K., Bougiatioti, A., Ramonet, M., Pierros, F., Michalopoulos, P., Liakakou, E., Solomos, S., Quehe, P.-Y., Delmotte, M., Gerasopoulos, E., Kanakidou, M., Mihalopoulos, N., 2021. Greenhouse gases (CO_2 and CH_4) at an urban background site in Athens, Greece: levels, sources and impact of atmospheric circulation. *Atmos. Environ.* 253, 118372. <https://doi.org/10.1016/j.atmosenv.2021.118372>.
- Etheridge, D.M., Steele, L.P., Francey, R.J., Langenfelds, R., 1998. L: atmospheric methane between 1000 A.D. and present: evidence of anthropogenic emissions and climatic variability. *J. Geophys. Res. Atmos.* 103 (D13), 15979–15993. <https://doi.org/10.1029/98JD00923>.
- European Environment Agency, 2021. EEA emission inventory report. Available from: <https://www.eea.europa.eu/publications/european-union-emission-inventory-report-1>.
- Forster, P., Ramaswamy, V., Artaxo, P., Bernsten, T., Betts, R., Fahey, D.W., Haywood, J., Lean, J., Lowe, D.C., Myhre, G., Nganga, J., Prinn, R., Raga, G., Schulz, M., Van Dorland, R., 2007. *Changes in Atmospheric Constituents and in Radiative Forcing Chapter 2*. Cambridge University Press, United Kingdom.
- Friedlingstein, P., Jones, M.W., O'Sullivan, M., Andrew, R.M., Bakker, D.C.E., Hauck, J., Le Quéré, C., Peters, G.P., Peters, W., Pongratz, J., Sitoh, S., Canadell, J.G., Ciais, P., Jackson, R.B., Alin, S.R., Anthoni, P., Bates, N.R., Becker, M., Bellouin, N., Bopp, L., Chau, T.T.T., Chevallier, F., Chini, L.P., Cronin, M., Currie, K.I., Decharme, B., Djeutchouang, L.M., Dou, X., Evans, W., Feely, R.A., Feng, L., Gasser, T., Gilfillan, D., Gkrizalis, T., Grassi, G., Gregor, L., Gruber, N., Gürses, Ö., Harris, I., Houghton, R.A., Hurtt, G.C., Iida, Y., Ilyina, T., Luijckx, I.T., Jain, A., Jones, S.D., Kato, E., Kennedy, D., Klein Goldewijk, K., Knauer, J., Korsbakken, J.I., Körtzinger, A., Landschützer, P., Lausvet, S.K., Lefèvre, N., Lienert, S., Liu, J., Marland, G., McGuire, P.C., Melton, J.R., Munro, D.R., Nabel, J.E.M.S., Nakaoka, S.-I., Niwa, Y., Ono, T., Pierrot, D., Poulter, B., Rehder, G., Resplandy, L., Robertson, E., Rödenbeck, C., Rosan, T.M., Schwingler, J., Schwingshackl, C., Séférian, R., Sutton, A.J., Sweeney, C., Tanhua, T., Tans, P.P., Tian, H., Tilbrook, B., Tubiello, F., van der Werf, G.R., Vuichard, N., Wada, C., Wanninkhof, R., Watson, A.J., Willis, D., Wiltshire, A.J., Yuan, W., Yue, C., Yue, X., Zaehle, S., Zeng, J., 2022. Global carbon budget 2021. *Earth Syst. Sci. Data* 14 (4), 1917–2005. <https://doi.org/10.5194/essd-14-1917-2022>.
- Gerasopoulos, E., Kouvarakis, G., Vrekoussis, M., Kanakidou, M., Mihalopoulos, N., 2005. Ozone variability in the marine boundary layer of the eastern Mediterranean based on 7-year observations. *J. Geophys. Res.* 110 (D15), D15309. <https://doi.org/10.1029/2005JD005991>.
- Gerasopoulos, E., Kouvarakis, G., Vrekoussis, M., Donoussis, C., Mihalopoulos, N., Kanakidou, M., 2006. Photochemical ozone production in the eastern Mediterranean. *Atmos. Environ.* 40 (17), 3057–3069. <https://doi.org/10.1016/j.atmosenv.2005.12.061>.
- Gerasopoulos, E., Amiridis, V., Kazadzis, S., Kokkalis, P., Eleftheratos, K., Andreae, M.O., Andreae, T.W., El-Askary, H., Zerefos, C.S., 2011. Three-year ground based measurements of aerosol optical depth over the eastern Mediterranean: the urban environment of Athens. *Atmos. Chem. Phys.* 11 (5), 2145–2159. <https://doi.org/10.5194/acp-11-2145-2011>.
- Gros, V., Tsigaridis, K., Bonsang, B., Kanakidou, M., Pio, C., 2002. Factors controlling the diurnal variation of CO above a forested area in Southeast Europe. *Atmos. Environ.* 36 (19), 3127–3135. [https://doi.org/10.1016/S1352-2310\(02\)00237-6](https://doi.org/10.1016/S1352-2310(02)00237-6).
- Hazan, L., Tarniewicz, J., Ramonet, M., Laurent, O., Abbatis, A., 2016. Automatic processing of atmospheric CO_2 and CH_4 mole fractions at the ICOS atmosphere thematic Centre. *Atmos. Meas. Tech.* 9 (9), 4719–4736. <https://doi.org/10.5194/amt-9-4719-2016>.

- ICOS RI, 2020. In: Laurent, O. (Ed.), ICOS Atmosphere Station Specifications V2.0. ICOS ERIC <https://doi.org/10.18160/GK28-2188> (September).
- IPCC, 2022. Available from: In: RY, Masson-Delmotte, B.Z., Zhai, V.P., Pirani, A., Connors, S.L., Péan, C., Berger, S., Caud, N., Chen, Y., Goldfarb, L., Gomis, M.L., Huang, M., Leitzell, K., Lonnoy, E., Matthews, J.B.R., Maycock, T.K., Waterfield, T., Yelekçi, O., Yu, R., Zhou, B., Masson-Delmotte, V. (Eds.), IPCC, 2022: Climate Change 2022. The Physical Science Basis. Summary for Policymakers. Cambridge University Press, Cambridge, United Kingdom and New York, NY, USA. http://www.klimamanifest-von-heligenroth.de/wp-content/uploads/2014/02/IPCC2013_WG1AR5_ALL_FINAL_S768_14Grad_mitTitelCover.pdf.
- Jackson, R.B., Saunio, M., Bousquet, P., Canadell, J.G., Poulter, B., Stavert, A.R., Bergamaschi, P., Niwa, Y., Segers, A., Tsuruta, A., 2020. Increasing anthropogenic methane emissions arise equally from agricultural and fossil fuel sources. *Environ. Res. Lett.* 15 (7), 071002. <https://doi.org/10.1088/1748-9326/ab9ed2>.
- Joos, F., Spahni, R., 2008. Rates of change in natural and anthropogenic radiative forcing over the past 20,000 years. *Proc. Natl. Acad. Sci. U. S. A.* 105 (5), 1425–1430. <https://doi.org/10.1073/pnas.0707386105>.
- Kanakidou, M., Mihalopoulos, N., Kindap, T., Im, U., Vrekoussis, M., Gerasopoulos, E., Dermitzaki, E., Unal, A., Koçak, M., Markakis, K., Melas, D., Kouvarakis, G., Youssef, A.F., Richter, A., Hatzianastassiou, N., Hilboll, A., Ebojio, F., Wittrock, F., von Savigny, C., Burrows, J.P., Ladstaetter-Weissenmayer, A., Moubasher, H., 2011. Megacities as hot spots of air pollution in the East Mediterranean. *Atmos. Environ.* 45 (6), 1223–1235. <https://doi.org/10.1016/j.atmosenv.2010.11.048>.
- Khalil, M.A.K., Rasmussen, R.A., 1983. Sources, sinks, and seasonal cycles of atmospheric methane. *J. Geophys. Res. Ocean* 88 (C9), 5131–5144. <https://doi.org/10.1029/JC088iC09p05131>.
- Khalil, M.A.K., Rasmussen, R.A., 1990. The global cycle of carbon monoxide: trends and mass balance. *Chemosphere* 20 (1–2), 227–242. [https://doi.org/10.1016/0045-6535\(90\)90098-E](https://doi.org/10.1016/0045-6535(90)90098-E).
- Lamarque, J.F., Shindell, D.T., Josse, B., Young, P.J., Cionni, I., Eyring, V., Bergmann, D., Cameron-Smith, P., Collins, W.J., Doherty, R., Dalsoren, S., Faluvegi, G., Folberth, G., Ghan, S.J., Horowitz, L.W., Lee, Y.T., MacKenzie, I.A., Nagashima, T., Naik, V., Plummer, D., Righi, M., Rumbold, S.T., Schulz, M., Skeie, R.B., Stevenson, D.S., Strode, S., Sudo, K., Szopa, S., Voulgarakis, A., Zeng, G., 2013. The atmospheric chemistry and climate model intercomparison project (ACCMIP): overview and description of models, simulations and climate diagnostics. *Geosci. Model Dev.* 6 (1), 179–206. <https://doi.org/10.5194/gmd-6-179-2013>.
- Lan, X., Nisbet, E.G., Dlugokencky, E.J., Michel, S.E., 2021. What do we know about the global methane budget? Results from four decades of atmospheric CH₄ observations and the way forward. *Philos. Trans. R. Soc. A Math. Phys. Eng. Sci.* 379 (2210). <https://doi.org/10.1098/rsta.2020.0440> 20200440.
- Lelieveld, J., Berresheim, H., Borrmann, S., Crutzen, P.J., Dentener, F.J., Fischer, H., Feichter, J., Flatau, P.J., Heland, J., Holzinger, R., Korrmann, R., Lawrence, M.G., Levin, Z., Markowicz, K.M., Mihalopoulos, N., Minikin, A., Ramanathan, V., de Reus, M., Roelofs, G.J., Scheeren, H.A., Sciare, J., Schlager, H., Schultz, M., Siegmund, P., Steil, B., Stephanou, E.G., Stier, P., Traub, M., Warneke, C., Williams, J., Ziereis, H., 2002. Global air pollution crossroads over the Mediterranean. *Science* (80-) 298 (5594). <https://doi.org/10.1126/science.1075457> 794 LP–799.
- Lelieveld, J., Gromov, S., Pozzer, A., Taraborrelli, D., 2016. Global tropospheric hydroxyl distribution, budget and reactivity. *Atmos. Chem. Phys.* 16 (19), 12477–12493. <https://doi.org/10.5194/acp-16-12477-2016>.
- Liakakou, E., Bonsang, B., Williams, J., Kalivitis, N., Kanakidou, M., Mihalopoulos, N., 2009. C₂-C₈ NMHCs over the eastern Mediterranean: seasonal variation and impact on regional oxidation chemistry. *Atmos. Environ.* 43 (35). <https://doi.org/10.1016/j.atmosenv.2009.07.067>.
- Lopez, M., Schmidt, M., Yver, C., Messenger, C., Worthy, D., Kazan, V., Ramonet, M., Bousquet, P., Ciais, P., 2012. Seasonal variation of N₂O emissions in France inferred from atmospheric N₂O and 222Rn measurements. *J. Geophys. Res. Atmos.* 117. <https://doi.org/10.1029/2012JD017703>.
- Lopez, M., Schmidt, M., Ramonet, M., Bonne, J.-L., Colomb, A., Kazan, V., Laj, P., Pichon, J.-M., 2015. Three years of semicontinuous greenhouse gas measurements at the Puy de Dôme station (central France). *Atmos. Meas. Tech.* 8, 3941–3958. <https://doi.org/10.5194/amt-8-3941-2015>.
- Lowry, D., Lanoisellé, M.E., Fisher, R.E., Martin, M., Fowler, C.M.R., France, J.L., Hernández-Paniagua, I.Y., Novelli, P.C., Sriskantharajah, S., O'Brien, P., Rata, N.D., Holmes, C.W., Fleming, Z.L., Clemitshaw, K.C., Zazzeri, G., Pommier, M., McLinden, C.A., Nisbet, E.G., 2016. Marked long-term decline in ambient CO mixing ratio in SE England, 1997–2014: evidence of policy success in improving air quality. *Sci. Rep.* 6 (January), 1–12. <https://doi.org/10.1038/srep25661>.
- Mermigkas, M., Topaloglou, C., Balis, D., Koukoulis, M.E., Hase, F., Dubravica, D., Borsdorff, T., Lorente, A., 2021. F_{tir} measurements of greenhouse gases over Thessaloniki, Greece in the framework of cocoon and comparison with s5p/tropomi observations. *Remote Sens.* 13 (17), 3395. <https://doi.org/10.3390/rs13173395>.
- Mihalopoulos, N., Stephanou, E., Kanakidou, M., Pilitsidis, S., Bousquet, P., 1997. Tropospheric aerosol ionic composition in the Eastern Mediterranean region. *Tellus Ser. B Chem. Phys. Meteorol.* 49B (3), 314–326. <https://doi.org/10.3402/tellusb.v49i3.15970>.
- Myriokefalitakis, S., Daskalakis, N., Fanourgakis, G.S., Voulgarakis, A., Krol, M.C., Aan de Brugh, J.M.J., Kanakidou, M., 2016. Ozone and carbon monoxide budgets over the eastern Mediterranean. *Sci. Total Environ.* 563–564, 40–52. <https://doi.org/10.1016/j.scitotenv.2016.04.061>.
- Potter, C.S., Klooster, S.A., Chatfield, R.B., 1996. Consumption and production of carbon monoxide in soils: a global model analysis of spatial and seasonal variation. *Chemosphere* 33 (6), 1175–1193. [https://doi.org/10.1016/0045-6535\(96\)00254-8](https://doi.org/10.1016/0045-6535(96)00254-8).
- Rigby, M., Montzka, S.A., Prinn, R.G., White, J.W.C., Young, D., O'Doherty, S., Lunt, M.F., Ganesan, A.L., Manning, A.J., Simmonds, P.G., Salameh, P.K., Harth, C.M., Mühle, J., Weiss, R.F., Fraser, P.J., Steele, L.P., Krummel, P.B., McCulloch, A., Park, S., 2017. Role of atmospheric oxidation in recent methane growth. *Proc. Natl. Acad. Sci.* 114 (21), 5373–5377. <https://doi.org/10.1073/pnas.1616426114>.
- Saunio, M.R., Stavert, A., Poulter, B., Bousquet, P.G., Canadell, J.B., Jackson, R.A., Raymond, P.J., Dlugokencky, E., Houweling, S.K., Patra, P., Ciais, P.K., Arora, V., Bastviken, D., Bergamaschi, P.R., Blake, D., Brailsford, G., Bruhwiler, L.M., Carlson, K., Carroll, M., Castaldi, S., Chandra, N., Crevoisier, C.M., Crill, P., Covey, K.L., Curry, C., Etiope, G., Frankenberg, C., Gedney, N.L., Hegglin, M., Höglund-Isaksson, L., Hugelius, G., Ishizawa, M., Ito, A., Janssens-Maenhout, G.M., Joos, F., Kleinen, T.B., Jensen, K., Krummel, P.L., Langenfelds, R.G., Laruelle, G., Liu, L., MacHida, T., Maksyutov, S.C., McDonald, K., McNorton, J.A., Miller, P.R., Melton, J., Morino, I., Müller, J., Murguía-Flores, F., Naik, V., Niwa, Y., Noce, S., O'Doherty, S.J., Parker, R., Peng, C., Peng, S.P., Peters, G., Prigent, C., Prinn, R., Ramonet, M., Regnier, P.J., Riley, W.A., Rosentretter, J., Segers, A.J., Simpson, I., Shi, H.J., Smith, S., Paul Steele, L.F., Thornton, B., Tian, H., Tohjima, Y.N., Tubiello, Tsuruta, A., Viovy, N., Tubiello, Y.N., Tohjima, F., Voulgarakis, A.S., Weber, T., Van Weele, M.R., Van Der Werf, G.F., Weiss, R., Worthy, D., Wunch, D., Yin, Y., Yoshida, Y., Zhang, W., Zhang, Z., Zhao, Y., Zheng, B., Zhu, Q., Zhu, Q., Zhuang, Q., 2020. The global methane budget 2000–2017. *Earth Syst. Sci. Data* 12 (3), 1561–1623. <https://doi.org/10.5194/essd-12-1561-2020>.
- Schmidt, M., Lopez, M., Yver Kwok, C., Messenger, C., Ramonet, M., Wastine, B., Vuillemin, C., Truong, F., Gal, B., Parmentier, E., Cloué, O., Ciais, P., 2014. High-precision quasi-continuous atmospheric greenhouse gas measurements at Trainou tower (Orléans forest, France). *Atmos. Meas. Tech.* 7, 2283–2296. <https://doi.org/10.5194/amt-7-2283-2014>.
- Schneisinger, O., Buchwitz, M., Reuter, M., Bovensmann, H., Burrows, J.P., Borsdorff, T., Deutscher, N.M., Feist, D.G., Griffith, D.W.T., Hase, F., Hermans, C., Iraci, L.T., Kivi, R., Landgraf, J., Morino, I., Notholt, J., Petri, C., Pollard, D.F., Roche, S., Shiomi, K., Strong, K., Sussmann, R., Velasco, V.A., Warneke, T., Wunch, D., 2019. A scientific algorithm to simultaneously retrieve carbon monoxide and methane from TROPOMI onboard Sentinel-5 precursor. *Atmos. Meas. Tech.* 12 (12), 6771–6802. <https://doi.org/10.5194/amt-12-6771-2019>.
- Sciare, J., Oikonomou, K., Favez, O., Liakakou, E., Markaki, Z., Cachier, H., Mihalopoulos, N., 2008. Long-term measurements of carbonaceous aerosols in the eastern Mediterranean: evidence of long-range transport of biomass burning. *Atmos. Chem. Phys.* 8 (18), 5551–5563. <https://doi.org/10.5194/acp-8-5551-2008>.
- Stern, N., 2007. The economics of climate change: the stern review. *Econ. Clim. Chang. Stern Rev.* 1–692. <https://doi.org/10.1017/CBO9780511817434.9780521877>.
- Voulgarakis, A., Naik, V., Lamarque, J.F., Shindell, D.T., Young, P.J., Prather, M.J., Wild, O., Field, R.D., Bergmann, D., Cameron-Smith, P., Cionni, I., Collins, W.J., Dalsøren, S.B., Doherty, R.M., Eyring, V., Faluvegi, G., Folberth, G.A., Horowitz, L.W., Josse, B., MacKenzie, I.A., Nagashima, T., Plummer, D.A., Righi, M., Rumbold, S.T., Stevenson, D.S., Strode, S.A., Sudo, K., Szopa, S., Zeng, G., 2013. Analysis of present day and future OH and methane lifetime in the ACCMIP simulations. *Atmos. Chem. Phys.* 13 (5), 2563–2587. <https://doi.org/10.5194/acp-13-2563-2013>.
- Walker, A.P., De Kauwe, M.G., Bastos, A., Belmecheri, S., Georgiou, K., Keeling, R.F., McMahon, S.M., Medlyn, B.E., Moore, D.J.P., Norby, R.J., Zaehle, S., Anderson-Teixeira, K.J., Battipaglia, G., Brienen, R.J.W., Canham, C.D., Canham, C.D., Campbell, E., Canadell, J.G., Ciais, P., Craig, M.E., Ellsworth, D.S., Farquhar, G.D., Faticchi, S., Fisher, J.B., Frank, D.C., Graven, H., Gu, L., Haverd, V., Heilmann, K., Heimann, M., Hungate, B.A., Iversen, C.M., Joos, F., Jiang, M., Keenan, T.F., Knauer, J., Körner, C., Leshyk, V.O., Leuzinger, S., Liu, Y., MacBean, N., Malhi, Y., McVicar, T.R., Penuelas, J., Pongratz, J., Powell, A.S., Riutta, T., Sabot, M.E.B., Schleucher, J., Sitch, S., Smith, W.K., Sulman, B., Taylor, B., Terrer, C., Torn, M.S., Treseder, K.K., Trugman, A.T., Trumbore, S.E., Mantgem, P.J., Voelker, S.L., Whelan, M.E., Zuidema, P.A., 2021. Integrating the evidence for a terrestrial carbon sink caused by increasing atmospheric CO₂. *New Phytol.* 229 (5), 2413–2445. <https://doi.org/10.1111/nph.16866>.
- Yver-Kwok, C., Philippon, C., Bergamaschi, P., Biermann, T., Calzolari, F., Chen, H., Conil, S., Cristofanelli, P., Delmotte, M., Hatakka, J., Heliasz, M., Hermansen, O., Kominková, K., Kubistin, D., Kumps, N., Laurent, O., Laurila, T., Lehner, I., Levula, J., Lindauer, M., Lopez, M., Mammarella, I., Manca, G., Marklund, P., Metzger, J.-M., Mölder, M., Platt, S.M., Ramonet, M., Rivier, L., Scheeren, B., Sha, M.K., Smith, P., Steinbacher, M., Vitková, G., Wyss, S., 2021. Evaluation and optimization of ICOS atmospheric station data as part of the labeling process. *Atmos. Meas. Tech.* 14 (1), 89–116. <https://doi.org/10.5194/amt-14-89-2021>.
- Zheng, B., Chevallier, F., Yin, Y., Ciais, P., Fortems-Cheiney, A., Deeter, M.N., Parker, R.J., Wang, Y., Worden, H.M., Zhao, Y., 2019. Global atmospheric carbon monoxide budget 2000–2017 inferred from multi-species atmospheric inversions. *Earth Syst. Sci. Data Discuss.* 1, 1–42. <https://doi.org/10.5194/essd-2019-61>.
- Zittis, G., Almazroui, M., Alpert, P., Ciais, P., Cramer, W., Dahdal, Y., Fnaiss, M., Francis, D., Hadjinicolaou, P., Howari, F., Jrrar, A., Kaskaoutis, D.G., Kulmala, M., Lazoglou, G., Mihalopoulos, N., Lin, X., Rudich, Y., Sciare, J., Stenchikov, G., Xoplaki, E., Lelieveld, J., 2022. Climate change and weather extremes in the Eastern Mediterranean and Middle East. *Rev. Geophys.* 60 (3), e2021RG000762. <https://doi.org/10.1029/2021RG000762>.